Inorganic Chemistry

pubs.acs.org/IC Article

Solvent-Induced Spin-State Change in Copper Corroles

Christopher M. Lemon,* Andrew G. Maher, Bryce L. Anderson, Eric D. Bloch, Michael Huynh, Abie L. McCollar, and Daniel G. Nocera*



Cite This: Inorg. Chem. 2022, 61, 20288–20298



ACCESS

Metrics & More

Article Recommendations

s Supporting Information

ABSTRACT: The electronic structure of copper corroles has been a topic of debate and revision since the advent of corrole chemistry. The ground state of these compounds is best described as an antiferromagnetically coupled Cu(II) corrole radical cation. In coordinating solvents, these molecules become paramagnetic, and this is often accompanied by a color change. The underlying chemistry of these solvent-induced properties is currently unknown. Here, we show that a coordinating solvent, such as pyridine, induces a change in the ground spin state from an antiferromagnetically coupled Cu(II) corrole radical cation to a ferromagnetically coupled triplet. Over time, the triplet reacts to produce a species with spectral signatures that are characteristic of the one-

Antiferromagnetic
Coupling: S = 0

Solvent-Induced Change in Spin State

Ferromagnetic
Coupling: S = 1

electron-reduced Cu(II) corrole. These observations account for the solvent-induced paramagnetism and the associated color changes that have been observed for copper corroles in coordinating solvents.

INTRODUCTION

Spin crossover is the process by which a coordination complex undergoes a binary switch in the molecular spin state. The vast majority of compounds that undergo spin crossover are (pseudo)octahedral complexes of first-row transition metals with d^4-d^7 configurations. The prototypical example of spin crossover is the low- to high-spin transition of octahedral Fe(II) complexes. Spin crossover molecules and materials continue in their prominence due to the applications of these complexes as molecular switches, logic gates, and qubits for quantum computing. $^{1,3-6}$

Spin crossover may be induced by a variety of external stimuli, including temperature, light, pressure, or magnetic field. However, solution-phase chemistry enables additional characterization of this phenomenon, as other methods of inducing a spin-state change are possible, such as the coordination of an exogenous ligand. Perturbations in the ligand environment can enable chemosensing applications of spin crossover.8 Ligand-induced spin-state switching has been popularized with Ni(II) porphyrins and subsequently chlorins and isobacteriochlorins. 10 In these complexes, the Ni(II) center switches from S = 0 to S = 1 upon coordination of an axial ligand. These molecules have been used for light-driven, coordination-induced spin-state switching, where the cis/trans photo-isomerization of an azopyridine controls the coordination of the axial ligand to the metal center. 11,12 This approach has been used to produce a photoswitchable contrast agent for magnetic resonance imaging. 13

While spin crossover and coordination-induced spin-state changes have been observed throughout the first-row transition metals, this phenomenon is unusual for copper complexes owing to the d^9 configuration of Cu(II), which unto itself

prohibits spin isomerization. However, the involvement of Cu(II) in a spin crossover system could be enabled with the utilization of redox non-innocent ligands. A prototypical example of ligand non-innocence for copper complexes is the corrole ligand. Theoretical studies have demonstrated that these compounds are best described as antiferromagnetically coupled Cu(II) corrole radical cations, the formulation of which has been unequivocally established experimentally. The ferromagnetically coupled triplet state is thermally accessible, but the barrier is prohibitively high (0.144 eV) for spin crossover to be achieved. Indeed, only 3.3% of the Cu(II) corrole radical cation resides in the triplet state at 100 °C. 21

Axial ligation provides a tool to overcome the high thermal barrier to triplet population. Indeed, the viability of this posit is indicated by the solvent-dependent behavior of copper corroles. The broadness of the signals in the 1H NMR spectrum of Cu(II) corroles increases in DMF- d_7 , and the samples are paramagnetic in pyridine- d_5 , as determined by the lack of proton signals in the -2 to 12 ppm range. Additionally, changes in the UV-vis absorption spectrum are observed in coordinating solvents (DMF, pyridine, and DMSO) and are accompanied by the appearance of EPR signals. Against this backdrop, we set out to understand the role that coordinating solvents, such as pyridine, play in modulating the electronic structure of copper corroles. Our

Received: July 26, 2022 Published: December 2, 2022





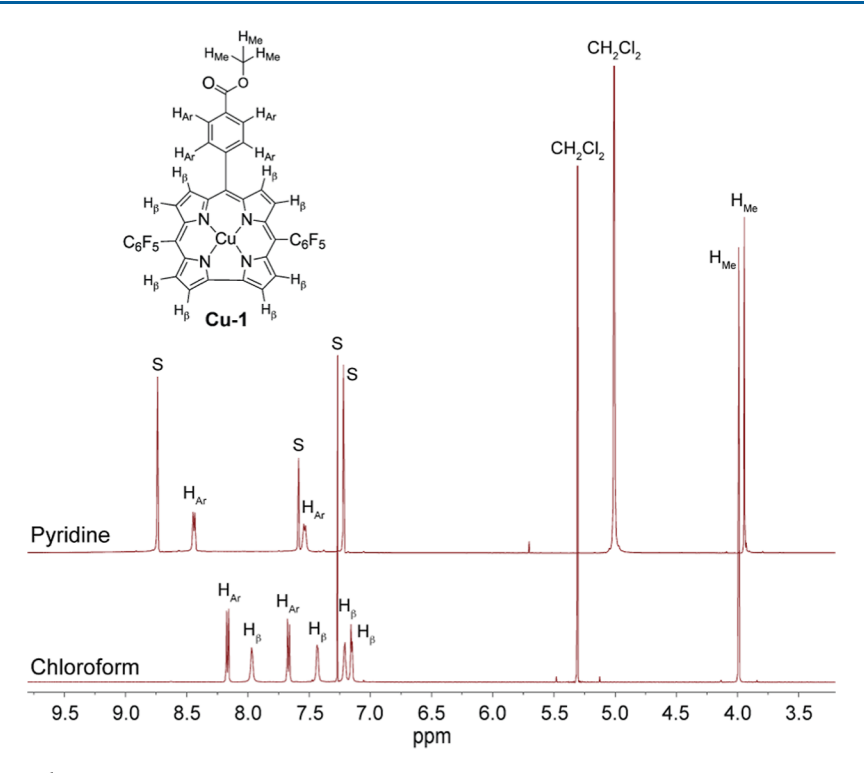


Figure 1. Comparison of the 1 H NMR spectrum of Cu-1 in pyridine- d_5 and CDCl₃. The peaks are annotated to correlate with the labeled structure: methyl ester protons (H_{Me}), aryl protons of the *meso* substituent (two resonances, H_{Ar}), β-pyrrole protons (four resonances, H_β), and residual deuterated solvent (S). For the spectrum in pyridine- d_5 , the four H_β signals have disappeared, suggesting that Cu-1 is paramagnetic in coordinating solvents.

results demonstrate that pyridine ligation induces spin-state switching in copper corroles, changing the ground state from an antiferromagnetically coupled singlet to a ferromagnetically coupled triplet, which then reacts to form the reduced corrole.

■ EXPERIMENTAL SECTION

Materials. The following materials were used as received: acetonitrile, pyridine, 2-methyl-tetrahyrdofuran (2-Me-THF), and toluene from Sigma-Aldrich and chloroform-d (CDCl₃) and pyridine- d_5 from Cambridge Isotope Laboratories. Tetrabutylammonium hexafluorophosphate ([TBA][PF₆]) from Sigma-Aldrich was recrystallized from EtOH and subsequently dried under vacuum prior to use. Acetonitrile (MeCN) from Sigma-Aldrich was obtained from a solvent drying system (Pure Process Technologies) and stored over 3 Å molecular sieves.

Synthesis of 10-(4-Methoxycarbonylphenyl)-5,15-*bis*-(pentafluorophenyl)corrolatocopper (Cu-1). The free-base corrole 10-(4-methoxycarbonylphenyl)-5,15-*bis*(pentafluorophenyl)corrole (H₃-1)²⁶ and its copper complex (Cu-1)²¹ were prepared according to literature methods. ¹H NMR (500 MHz, pyridine- d_5 , 23 °C) 3.94 (s, 3H), 7.54 (d, J = 7.7 Hz, 2H), 8.44 (d, J = 7.7 Hz, 2H). No β -pyrrole protons were observed for this sample. ¹H NMR (500 MHz, CDCl₃, 23 °C) 3.98 (s, 3H), 7.14 (bd, J = 4.6 Hz, 2H), 7.21 (bd, J = 4.0 Hz, 2H), 7.42 (bd, J = 4.0 Hz, 2H), 7.65 (d, J = 8.0 Hz, 2H), 7.97 (br s, 2H), 8.16 (d, J = 8.0 Hz, 2H).

Physical Methods. NMR spectra were recorded on a Varian Inova-500 NMR spectrometer at the Harvard University Department of Chemistry and Chemical Biology Laukien-Purcell Instrumentation Center and internally referenced to the residual solvent signal (δ = 7.26 for CDCl₃ or δ = 7.22 for pyridine- d_5). Experiments performed at the Montana State University Chemistry and Biochemistry NMR Center utilized a Bruker 500 MHz Ascend AVANCE III HD spectrometer. UV—vis absorption spectra were acquired using a Cary 5000 spectrometer (Agilent) or a Shimadzu UV-3101PC spectrometer. Perpendicular-mode X-band EPR spectra were recorded on a Bruker ElexSys E500 with an ER4112 SHQE-W resonator or a Bruker

E580 with an MD5 resonator. Spectra were recorded at 77 K using a liquid nitrogen dewar.

Femtosecond transient absorption (TA) spectra were acquired using a Libra-F-HE (Coherent) chirped-pulse amplified Ti/sapphire laser system. Methods for acquiring and processing TA data have been previously described. Phe 800 nm laser output was then used to pump an OperA Solo (Coherent) optical parametric amplifier (OPA) to generate excitation pulses of 400 nm that were attenuated to $2-5~\mu\text{J}$ per pulse at the sample using neutral density filters. Air-free corrole samples for ultrafast TA spectroscopy were prepared using three cycles of freeze–pump–thaw (FPT) to pressures below 10^{-4}

Electrochemical measurements were made in a glovebox under a nitrogen atmosphere with a CH Instruments 760D electrochemical workstation using CHI Version 10.03 software. Samples were prepared at concentrations of ~1 mM in acetonitrile with 0.1 M [TBA][PF₆] as the supporting electrolyte. Cyclic voltammograms (CVs) were recorded at a scan rate of 100 mV/s using a glassy carbon button working electrode, a Ag wire reference electrode, and a Pt wire counter electrode. The CVs were internally referenced to ferrocene. Thin-layer UV-vis spectroelectrochemistry experiments were performed using a 0.5 mm path length quartz cell with an Ocean Optics USB4000 spectrophotometer and DT-Mini-2GS UV-vis-NIR light source in conjunction with the CH electrochemical workstation described above. Samples were prepared at ~0.2 mM of compound with 0.1 M [TBA][PF₆] in acetonitrile. Bulk electrolysis was performed using a Pt flag working electrode, a Ag wire reference electrode, and a Pt wire counter electrode.

Magnetic measurements were recorded using a Quantum Design MPMS 7AC SQUID magnetometer. Solution-based susceptibility measurements were made for the compound in pyridine. The sample was sealed in an NMR tube under vacuum. DC magnetic susceptibility data were collected over the 2–298 K range at a field of 3.5 T. The magnetic susceptibilities of the compound were adjusted for diamagnetic contributions using the constitutive

corrections from Pascal's constants. 30 All data were fit 31 to the following Hamiltonian

$$\hat{H} = -J\hat{S}_{A} \bullet \hat{S}_{B} + \beta(\hat{S}_{A} \bullet g_{A} + \hat{S}_{B} \bullet g_{B}) \bullet B$$
(1)

where J is the exchange coupling constant, \hat{S} is the spin angular momentum operator, β is the Bohr magneton of the electron, g is the electron g-factor, and B is the applied field; the subscripts A and B refer to the two spin components that are coupled. This Hamiltonian accounts for both magnetic exchange (first term) and Zeeman splitting (second term). Solution magnetic moments were also determined with the Evans method, $^{32,33}_{32,33}$ using a coaxial NMR tube. A solution of the compound was prepared in pyridine- d_5 and spiked with MeCN, which served as the indicator. The interior tube was filled with a comparable concentration of MeCN in pyridine- d_5 . NMR spectra were recorded on a Varian Inova-500 NMR spectrometer at 23 °C. Diamagnetic corrections were estimated using Pascal's constants.

Computational Details. Density functional theory (DFT) calculations were performed with the hybrid functional Becke-3 parameter exchange functional 34-36 and the Lee-Yang-Parr nonlocal correlation functional (B3LYP), ³⁷ as implemented in the Gaussian 09, Revision D.01 software package.³⁸ For light atoms (H, C, N, O, and F), a polarized split-valence triple- ζ basis set that includes p functions on hydrogen atoms and d functions on other atoms [i.e., the 6-311G(d,p) or 6-311G** basis set] was used. A Dirac-Fock^{39,40} relativistic effective core potential (i.e., MDF10) was used for Cu. All calculations were performed with a conductor-like polarizable continuum solvation model (CPCM) in toluene. 41,42 All geometries were confirmed as local minima structures by calculating the Hessian matrix and ensuring that no imaginary eigenvalues were present. Excited-state calculations were performed using time-dependent DFT (TD-DFT)⁴³⁻⁴⁷ with the same functionals, basis sets, and solvation details as the ground state, but with the inclusion of diffuse functions on all light atoms (i.e., the 6-311++G** basis set). Excited-state energies were computed for the 40 lowest excited states. All optimized geometries, spin density plots, molecular orbitals, and simulated UVvis spectra (broadened with Gaussian functions with a half width of 0.15 eV) were generated in the program Gauss View 5.

RESULTS

NMR Experiments. The ¹H NMR spectrum of Cu-1 was recorded in pyridine- d_5 (Figure 1), as it has been previously demonstrated that Cu corroles exhibit paramagnetic behavior in that solvent.²⁵ Under these conditions, Cu-1 becomes paramagnetic, as demonstrated by the disappearance of the β pyrrole protons compared to the compound in CDCl₃ (Figure 1). Resonances from these protons could not be identified in the -105 to +115 ppm region; presumably, the signals are so broad that they cannot be readily distinguished from the baseline. Only the meso aryl and methyl ester signals are present, suggesting that the copper center has affected the signals of all nuclei adjacent to it (*i.e.*, the β -pyrrole protons). The 10-aryl substituent signals are perturbed to a lesser degree, due to the greater distance from the paramagnetic metal center. In an effort to detect the β -pyrrole protons, a variety of NMR experiments (e.g., variable field, COSY, HSQC, NOESY, and ROSEY) were performed, but the β -pyrrole signals were not observed. However, low-temperature experiments revealed several weak and broad signals that could be attributed to the β -pyrrole protons (Figure S1). Additionally, a variable temperature (VT) ¹H NMR experiment was performed for Cu-1 in pyridine-d₅ over the 25 to 95 °C range in an attempt to access a low-lying singlet state (Figure S2). However, the formation of a diamagnetic species was not observed at elevated temperatures. The shifting and broadening of the 10aryl protons are consistent with previous observations^{21,48} and

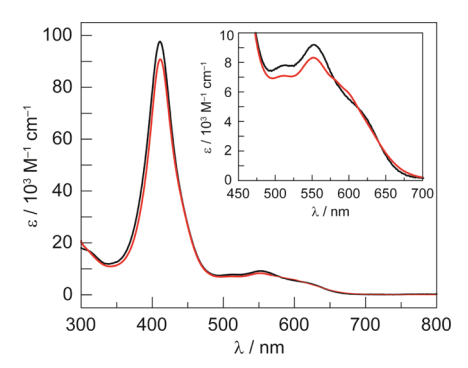


Figure 2. UV-vis absorption spectrum of **Cu-1** in toluene [—(black)] and pyridine [—(red)]. Inset: Expansion of the Q band region of the spectrum.

are attributed to faster ring rotation with increasing temperature. 48

Steady-State and Transient Optical Studies. The steady-state absorption spectrum of Cu-1 was recorded in toluene and pyridine (Figure 2). Based on literature reports, 23,24 it was expected that substantial changes would be observed in a coordinating solvent. Instead, the spectra of Cu-1 in toluene and pyridine are virtually identical; only nominal differences are observed in the Q-band region (Figure 2 inset). A titration of Cu-1 with pyridine was performed in chloroform. No shifts in the bands or appearance of new features was observed in the range of 2.5 to 512 equivalents of added pyridine (Figure S3a). This indicates that pyridine binding does not perturb the absorption spectrum of Cu-1. Indeed, no spectral changes were observed with 68,000 equivalents of added pyridine (Figure S3b). The absorption spectrum of Cu-1 in pyridine is unchanged over the course of 1 week (Figure S4); the sample remains a dark red-brown solution. However, after approximately 1 month, the bulk solution turns British racing green, and the spectrum shows the presence of a new species (Figure S5).

Ultrafast transient absorption (TA) spectroscopy of Cu-1 was examined to determine if the excited-state absorption properties were similarly insensitive to the solvent. A sample of Cu-1 in toluene was excited with 400 nm light (Figure 3). Analogous data for a sample of Cu-1 in toluene/pyridine are provided in Figure S6. It was found that two distinct spectral features evolve on different timescales. At fast timescales (t <20 ps, Figure 3A), a prominent feature at \sim 610 nm is observed and vanishes in 20 ps. Additionally, there is a feature at ~440 nm, which decays over the course of 500 ps (Figure 3B). Figure 3B clearly shows the bleach of the Q bands in the 475– 675 nm region. These observations are consistent with a previous study that reported ultrafast TA spectra of an A2B meso-triaryl copper corrole. 49 Similar growth and decay features are observed for Cu-1 in toluene/pyridine and evolve on similar timescales. Analysis of the kinetic data is provided in Figure S7, and the data are summarized in Table 1. The fast (610 nm) feature has a lifetime of 0.85 ps in toluene and 1.1 ps in toluene/pyridine. The slower feature (438 nm) exhibits biexponential kinetics that are the same within experimental error, with or without pyridine: ~ 140 ps (35%) and ~ 20 ps (65%). The kinetics of this process are consistent with a previously reported copper corrole: $7.0 \times 10^9 \text{ s}^{-1}$ or 140 ps. 49 Cu-1 exhibits faster decay kinetics relative to Cu porphyrins, which decay in ~450 ps. 50-52 This is because of the increase in the number of states due to the removal of

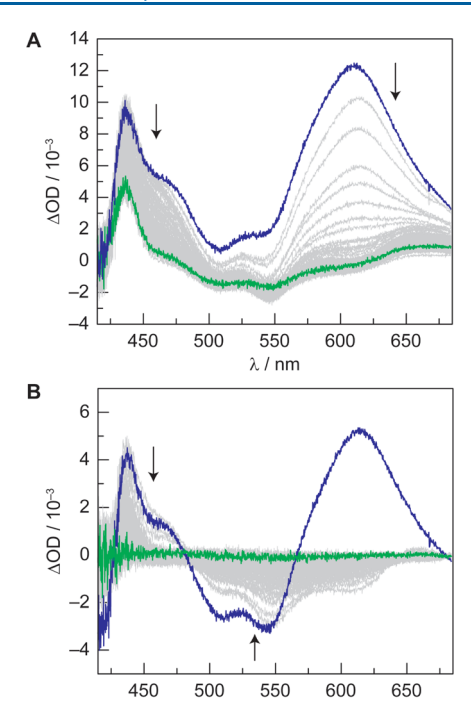


Figure 3. Ultrafast transient absorption (TA) spectra of a freeze–pump–thawed sample of Cu-1 in toluene ($\lambda_{\rm ex}=400$ nm). (A) Spectral evolution from the prompt spectrum [—(blue)] to a 20 ps delay [—(green)] in 0.2 ps increments. (B) Spectral evolution from the prompt spectrum [—(blue)] to a 500 ps delay [—(green)] in 5 ps increments.

 λ / nm

Table 1. Transient Absorption (TA) Kinetic Data for Cu-1

solvent	data (ps)	τ_1 (ps)	$A_1 (\%)^a$	τ_2 (ps)	$A_2 (\%)^a$
toluene	$0-20^{b}$	0.85 ± 0.04^{c}	100		
tol/pyr	$0-20^{b}$	1.10 ± 0.06	100		
toluene	$0-500^{d}$	138 ± 17	38	23.8 ± 5.8	62
tol/pyr	$0-500^{d}$	144 ± 18	31	20.2 ± 4.8	69

"Relative contribution to the biexponential fit. ^bMonitoring the feature at 610 nm (Figure 3A). ^cErrors reflect the error of the exponential fit. ^dMonitoring the feature at 438 nm (Figure 3B).

degeneracy, as a consequence of the lower symmetry of the corrole. Overall, as observed by steady-state spectroscopy, pyridine has little to no effect on the ultrafast TA spectra and dynamics of Cu-1.

Electrochemistry. Cyclic voltammograms of **Cu-1** in the absence and presence of pyridine are presented in Figure 4. Beginning at the open circuit potential and scanning cathodically, in the absence of pyridine, two reversible reductions at -0.28 and -2.15 V *versus* Fc⁺/Fc are observed followed by a reversible oxidation at +0.55 V and a quasi-reversible oxidation around +1.27 V (Figure S8). In the presence of pyridine, the oxidation event at +0.55 V becomes irreversible. Due to the irreversibility of this wave, additional features are observed on the return scan.

To gain additional insight into these redox processes, spectroelectrochemical experiments were performed. As expected from the CVs, the first reduction is unaffected by pyridine (Figure S9). However, the spectra for the oxidation (+0.8 V) are significantly different in the presence and absence of pyridine (Figure S10). While the Soret intensity decreases in both cases, the intensity of the Q bands increases when

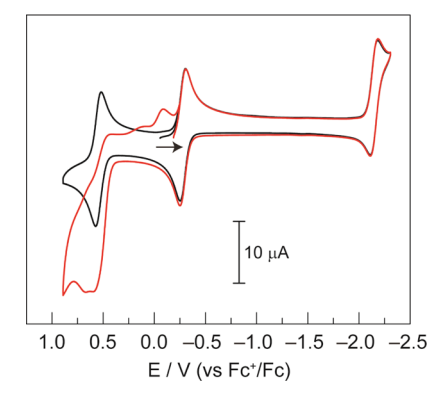


Figure 4. Cyclic voltammogram of **Cu-1** in MeCN with 0.1 M $[TBA][PF_6]$ recorded at 100 mV/s with [-(red)] and without [-(black)] added pyridine.

pyridine is present. Given the irreversibility of the oxidation with added pyridine, it is unclear whether this spectrum represents the oxidized species itself or products from subsequent chemical reactivity.

Magnetometry. Solution-based susceptibility data were collected to determine the effect of pyridine on the magnetic properties of Cu-1. A saturated solution (20+ mg/mL) of Cu-1 in pyridine was sealed under vacuum. A fraction of the material dissolved in solution with the bulk of the compound remaining as a solid. The magnetic moment of this sample (Figure 5A, blue circles) was recorded as a function of temperature at 3.5 T in order to draw direct comparisons to antiferromagnetic Cu-1. For the heterogeneous sample, the data were fit to a linear combination of two non-interacting species, each with the Hamiltonian described in eq 1. The fit yields 80% antiferromagnetic Cu-1²¹ and 20% of a S = 1species, which is readily observed in the curvature of the data at T < 50 K. Although obscured by the solid sample of Cu-1, it is noteworthy that an S = 1 signal is observed. Over the course of several weeks, the sample turned from brown to green and the susceptibility was remeasured (Figure 5A, green squares). It was found that the susceptibility was in accordance with an S = 1/2 species, indicative of a typical paramagnet. The decrease in γT at low temperature (<15 K) is consistent with magnetic ordering, given the high concentration of the sample. This phenomenon was also observed for a related Cu(II) isocorrole $(S = 1/2)^2$

Conversion of Cu-1 in pyridine to a species with S=1 is better supported by the Evans method. Figure 5B shows a plot of the susceptibility of Cu-1 in pyridine- d_5 as a function of time. For a freshly prepared sample, the measured value of $\mu_{\rm eff}=2.88$ BM is consistent with the calculated value of 2.83 BM for a triplet (S=1). Over the course of 4 weeks, the magnetic moment of this sample deceases to 1.77 BM, which is similar to the calculated value of 1.73 BM for a doublet (S=1/2). These data clearly show that Cu-1 in pyridine begins as a triplet (S=1) and slowly converts to a doublet over time (S=1/2).

EPR Experiments. EPR studies support the findings of the Evans method. A freshly prepared sample of **Cu-1** in a glovebox with rigorously dry solvents (1:1 pyridine/2-Me-THF) does not display an EPR signal. The absence of an EPR signal is consistent with an S=1 species, as triplet states are usually not readily observed by EPR in standard perpendicular mode. Safter several months, the sample, which was stored under vacuum and in the dark, turns from brown to British

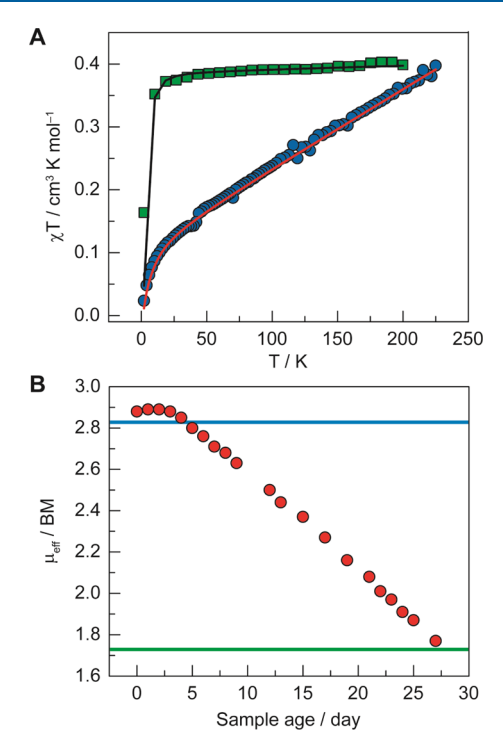


Figure 5. (A) SQUID data for a solution sample of Cu-1 in pyridine. The fresh, heterogeneous sample [●(blue)] fits to a mixture of solid Cu-1 (80%) and a species with S = 1 (20%). After several weeks, the sample turned green and was remeasured [■(green)]. These data show that the compound is now a doublet (S = 1/2). (B) Magnetic moment of Cu-1 in pyridine- d_S as a function of time, as measured by the Evans method (recorded at 23 °C). For a fresh sample, the magnetic moment is 2.88 BM, which is close to the theoretical value of 2.83 BM for S = 1 [—(blue)]. Over the course of 4 weeks, the magnetic moment decreases to 1.77 BM, which is close to the theoretical value of 1.73 BM for S = 1/2 [—(green)].

racing green. The EPR spectrum for this sample (Figure 6) is characteristic of an axial doublet for a single unpaired electron

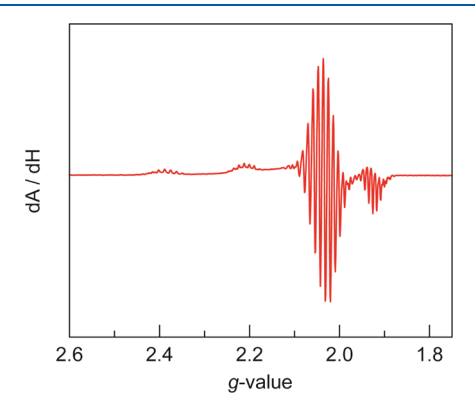


Figure 6. X-band EPR spectrum of Cu-1 in 2-Me-THF/pyridine after several months, recorded at 77 K. The spectrum shows one unpaired electron that exhibits hyperfine coupling to the ^{65/63}Cu nucleus and ligand superhyperfine coupling to the four ¹⁴N nuclei.

(S = 1/2) with hyperfine coupling to the ⁶⁵Cu/⁶³Cu nucleus (I = 3/2) to give a four-line pattern; this signal is further split by ligand superhyperfine coupling to the four ¹⁴N nuclei (I = 1) of the corrole core to give a nine-line pattern. Given the sharp signals and the similarity of the spectrum to an analogous Cu(II) isocorrole, ²¹ this signal is consistent with an S = 1/2

species, which is substantiated by magnetometry. We note that this EPR signal is obtained from Cu-1 more immediately if benchtop solvents with adventitious water are used for sample preparation (Figure S11). Presumably, trace water accelerates the formation of the species that gives rise to the doublet EPR signal.

Density Functional Theory Calculations. DFT calculations were performed to determine the ground spin state of Cu-1 upon coordination of an axial pyridine ligand, Cu-1-pyr. Three different spin scenarios were examined: a spin-restricted singlet, a spin-unrestricted triplet, and a spin-unrestricted, broken symmetry singlet. These scenarios correspond to a closed shell Cu^{III}, a ferromagnetically coupled Cu^{II} corrole radical cation (3CuII), and an antiferromagnetically coupled Cu^{II} corrole radical cation (¹Cu^{II}). These calculations were performed using the B3LYP functional with the 6-311G(d,p) basis set and a CPCM solvation model in toluene (Tables S1-S3 and Figures S12 and S13). These calculations indicate that ³Cu^{II} is the lowest energy configuration, with the ¹Cu^{II} and ¹Cu^{III} structures +0.008 and +0.212 eV higher in energy, respectively. Moreover, the triplet-state calculation predicts the shortest Cu-N_{pyr} distance of 2.506 Å, a value that is similar to that observed for the solid-state structure of a Cu(II) porphyrin with a single axial pyridine ligand $[d(Cu-N_{pyr})]$ = 2.38 Å].⁵⁴ The ¹Cu^{II} and ¹Cu^{III} calculations give longer Cu- N_{pyr} distances of 2.586 and 2.854 Å, respectively.

Figure 7 shows the calculated spin density plots for singlet Cu-1 and triplet Cu-1·pyr, as well as qualitative frontier molecular orbital diagrams; the canonical a2 and b1 ligand orbitals are included for reference. As previously determined, 21 Cu-1 is an antiferromagnetically coupled Cu(II) corrole radical cation. The spin density plot (Figure 7B) shows one α electron (blue) in the Cu $d_{x^2-y^2}^{\frac{1}{2}}$ orbital and one β electron (green) delocalized over the corrole ligand, which maps the shape of the b₁ orbital. For the pyridine adduct Cu-1·pyr, the spin density plot (Figure 7C) shows one α electron in $d_{x^2-y^2}$ and one α electron delocalized over the corrole ligand, corresponding to the shape of the b₁ orbital. The spin density plot of Cu-1.pyr is nearly identical to that of Cu-1; the only difference between the two plots (Figure 7B,C) is a spin flip for the electron delocalized over the ligand. As a result, the adduct is best described as a ferromagnetically coupled Cu(II) corrole radical cation.

TD-DFT methods were used to predict the electronic transitions for Cu-1·pyr. Calculations were performed using the same functional, basis set, and solvation model as the ground state, but with the inclusion of diffuse functions on all light atoms [i.e., the 6-311++G(d,p) basis set]. The major Q and Soret transitions for the pyridine adduct Cu-1·pyr (Figure S14 and Table S4) are only 0.02–0.06 eV different from Cu-1,²¹ paralleling the experimental observation that pyridine coordination has a nominal effect on the optical properties of Cu-1 (Figure S15).

DISCUSSION

Like porphyrins, corroles are aromatic tetrapyrrole macrocycles with 18 π -electrons in the main conjugation pathway, but with a contracted 23-atom core due to a direct pyrrole—pyrrole linkage. When fully deprotonated, the corrole macrocycle is a trianionic ligand, making it ideal for coordinating the formal +3 charge of metal centers. However, if the +3 state is more oxidizing than the corrole macrocycle, then ligand redox

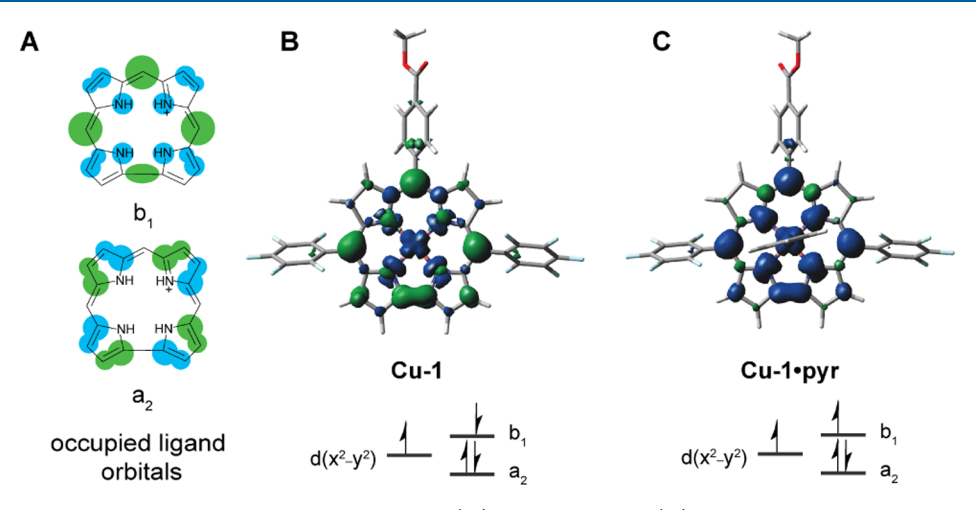


Figure 7. (A) Canonical occupied corrole ligand orbitals: HOMO (b_1) and HOMO-1 (a_2), adapted from ref 26. To illustrate the electronic structure of each derivative examined in this study, the calculated spin density plot and corresponding orbital occupancy (*i.e.*, qualitative MO diagram) are provided for (B) singlet Cu-1 and (C) triplet Cu-1-pyr.

non-innocence will result. 57,58 This is the case for Cu corroles, where the ground state is best described as a Cu(II) corrole radical cation, with antiferromagnetic coupling between the metal and macrocycle spins. 14,21,22 This study demonstrates that the coupling can be modulated by axial ligation. The ground state of the pyridine adduct Cu-1 pyr is a ferromagnetically coupled Cu(II) corrole radical cation. This assignment is supported by the identification of a paramagnetic species by ¹H NMR and the assignment of the spin state as S = 1 using the Evans method. Based on this suite of experiments, we conclude that the role of pyridine is to change the coordination environment and, consequently, the electronic structure of the complex to give a ground-state triplet. The change in the spin state of Cu-1 upon pyridine binding is analogous to a recent report of a tripodal V(II) complex, where ligand coordination results in a doublet ground state instead of a quartet (typical of d³ complexes).⁵⁹ Ligand binding results in a change in spin state due to ligand non-innocence and significant metal-ligand covalency, which is extant for both the V(II) complex and Cu-1.

The corrole core is inherently more electron-rich than the porphyrin macrocycle, ⁶⁰ making it more susceptible to decomposition. The inclusion of strongly electron-withdrawing pentafluorophenyl substituents helps to offset this electron density. Indeed, 5,10,15-tris(pentafluorophenyl)corrole is one of the most stable corroles, resisting decomposition under prolonged exposure to light and oxygen. ⁶¹ We have selected H₃-1 as the corrole of choice for our studies because it contains two pentafluorophenyl substituents for stability while providing a synthetic handle for further derivatization. The use of Cu-1 allows direct comparison to our previous study. ²¹ Additionally, the protons on the 10-aryl substituent enable ¹H NMR signals to be observed when studying Cu-1 in pyridine (Figure 1)

The change in the spin state of Cu-1 in pyridine is attributed to pyridine coordination at the metal center. It is unlikely that the solvent properties alone (e.g., dielectric constant or viscosity) could modulate the electronic structure of the molecule. Ligand binding changes the symmetry and coordination environment of the metal and, consequently, the relative energies of the frontier orbitals, resulting in an electron configuration that is distinct from the unbound molecule. We presume that one pyridine molecule is

coordinating, as observed in a previously reported crystal structure of a copper porphyrin (Figure S16).⁵⁴ To the best of our knowledge, this is the only structurally characterized example of a copper porphyrinoid with an axial pyridine ligand. The porphyrin exhibits a highly distorted, saddled conformation, creating a pocket that binds a second, non-coordinating pyridine molecule. The nitrogen atom of this second pyridine molecule is directed away from the metal center. These results suggest that Cu(II) tetrapyrroles may prefer to bind a single axial pyridine ligand, even in the presence of excess pyridine. For this reason, calculations were performed on Cu-1 with one pyridine ligand.

In order to validate the coordination environment of the copper center, attempts were made to crystallize Cu-1 with added pyridine, utilizing the same conditions that yielded diffraction-quality crystals of Cu-1. Additionally, efforts were made to crystallize the green reaction mixture. In both cases, the resultant crystals were of poor quality and did not diffract. Although the Cu-1 triplet is stable for several days, it undergoes a chemical transformation over the course of weeks (Figure 5B), which is the same timescale as crystal growth. Since the crystallization solution is changing daily, it is not surprising that diffraction-quality crystals could not be obtained.

Although pyridine coordination results in a change in spin state, there is not an accompanying change in the optical properties of Cu-1. This observation is supported by steadystate and ultrafast time-resolved optical spectroscopy, in conjunction with TD-DFT calculations. This is in contrast to cobalt corroles, where pyridine binding results in a significant change in the UV-vis absorption spectrum with a concomitant change in the electronic structure. 62 Five-coordinate pyridine adducts of Co corroles are yellow-brown in solution with noninnocent corrole ligands (i.e., antiferromagnetically coupled Co(II) corrole radical cations).⁶² Other five-coordinate Co corroles have been characterized that exhibit ligand noninnocence with neutral donor ligands: PPh₃⁶³ and DMSO.^{64–66} Conversely, six-coordinate di-pyridine adducts are emerald green in solution and are Co(III) species with innocent corrole ligands.⁶² Unlike Co corroles, pyridine coordination to Cu-1 results in a change in spin coupling between the metal and ligand, rather than a switch between an innocent and non-innocent corrole macrocycle.

In principle, it is expected that changes in the absorption spectrum should be observed upon pyridine binding. However, the observed bands arise from corrole-based π to π^* transitions; direct spectral signatures of the copper center are not observed. Additionally, the Cu $d_{x^2-y^2}$ orbital mixes with the corrole frontier orbitals to broaden these ligand-based transitions, obscuring any minor changes that might be observed upon pyridine binding. However, we note that the most significant difference in the absorption spectra is the shoulder on the red side of the lowest energy Q band (see the Figure 2 inset). The absorption maximum of this feature shifts from ~625 nm in toluene to ~600 nm in pyridine; this could represent a spectral signature of pyridine binding. Since no spectral changes were observed with 68,000 equivalents of pyridine (Figure S3b), this spectral shift may reflect the change in solvent dielectric. It should be noted that the structurally characterized pyridine adduct of a Cu(II) porphyrin (vide supra, Figure S16) does not exhibit significant changes in the absorption spectrum upon pyridine coordination. Consequently, it may not be surprising that pyridine binding does not perturb the optical properties of Cu-1.

Although pyridine does not significantly affect the absorption spectrum of Cu-1, the energy of the frontier molecular orbitals does change upon pyridine binding (Figure S17). The copper $d_{x^2-y^2}$ orbital is highly mixed with the ligand orbitals, 18-1 complicating the molecular orbital picture. For antiferromagnetically coupled Cu-1, the α HOMO-1 and β LUMO+2 orbitals have significant $d_{x^2-y^2}$ orbital character, and both orbitals increase in energy when pyridine is bound. The most significant energy difference is observed for the α LUMO and β HOMO, which change by -1.14 and +1.49 eV, respectively, for the pyridine adduct. The change in molecular orbital energies necessitates a change in the energy of the corresponding states. Since the triplet state of the Cu-1 pyridine complex is lower in energy than the singlet state, factors such as exchange energy and electron correlation, which would reduce electron-electron repulsion and favor a high spin state, may be significant. The simplified MO diagram in Figure 7 is a concise summary to illustrate the apparent orbital occupancy based on experimental and computational results.

While the triplet state is the lowest energy configuration for the pyridine adduct, DFT calculations predict that the singlet state is only 0.008 eV higher in energy. This energy gap is 50% smaller than that calculated for antiferromagnetic Cu-1 using the same computational methods (0.016 eV).²¹ It should be noted that these methods underestimate the experimental singlet-triplet energy gap for antiferromagnetic Cu-1: 0.144 eV by VT NMR or 0.153 eV by SQUID magnetometry.²¹ Given the smaller predicted energy gap for Cu-1 in pyridine, it is expected that a thermally accessible singlet state could be observed by VT NMR spectroscopy, but the formation of a diamagnetic species was not detected at elevated temperatures (Figure S2). However, the absence of a spectral signature for the singlet excited state may not be unexpected because the signal from a small amount of a diamagnetic species would be significantly broadened by the paramagnetic S = 1 species.

The pyridine adduct is a stable triplet that persists in solution for several days (Figure 5B) and does not exhibit an EPR signal (in standard perpendicular mode). Slowly, over the course of several weeks, the corrole undergoes a chemical transformation to yield a green species with S = 1/2 (Figure 5) and a well-resolved EPR spectrum (Figure 6). This product is assigned to be $[Cu-1]^-$, as the UV—vis absorption and EPR

spectra are consistent with the reduced derivative Zn[Cu-1]₂ (Figure S18).²¹ The formation of the one-electron reduced corrole in coordinating solvents has been previously observed.^{24,67} In these reports, the copper corroles bear electron-donating *meso* substituents (*e.g.*, 4-chlorophenyl or 2,4-dichlorophenyl), and the conversion to the reduced corrole is complete after 5 min, as measured by UV—vis absorption spectroscopy.²⁴ Conversely, the formation of [Cu-1]⁻ occurs slowly over weeks. The strongly electron-withdrawing pentafluorophenyl groups appear to help stabilize the triplet state, giving rise to the slow kinetics for the formation of the reduced species.

While the spectral signatures (absorption, EPR, and magnetometry) of the green species are consistent with the one-electron reduced corrole, an open question is the mechanism by which this species is formed. Based on the Evans data of Figure 5B, the linear plot indicates zeroth-order kinetics for the rate-determining step of the reduction process. This suggests that one component of this reaction is present in excess (e.g., pyridine or glass wall). We hypothesize that two mechanisms are possible: (1) reduction mediated by an unidentified molecule or (2) disproportionation of the triplet. For the reactivity-based reduction process, one potential molecule that could mediate this transformation is water. An EPR signal for [Cu-1] is observed for a freshly prepared sample using wet benchtop solvents (Figure S11). It should be noted that [Cu-1] is a minority species in this case, as the bulk sample remains red-brown instead of green. It appears that the pyridine adduct may serve as an oxidant that oxidizes some species in the sample to result in the formation of [Cu-1]. Such a mechanism has potential catalytic implications. Although a variety of metallocorroles have been utilized as electrocatalysts for small-molecule activation, ⁶⁸ copper corroles have only been used for proton reduction (i.e., hydrogen evolution).69-71 Although copper corroles cannot mediate electrocatalytic water oxidation,⁷² the change in electronic structure from the addition of a coordinating solvent could potentially enable oxidation catalysis with these molecules. Indeed, ligand non-innocence in mononuclear copper complexes has been leveraged for challenging reactions, such as water oxidation.⁷³ The quasi-reversible, putative twoelectron oxidation wave at +0.55 V (vs Fc⁺/Fc) for Cu-1 in pyridine (Figure 4) could be an additional advantage of copper corrole-catalyzed oxidation reactions.

An alternative mechanism for the formation of [Cu-1] in pyridine could be disproportionation of the triplet, yielding one equivalent of both the oxidized and reduced corrole: [Cu-1]⁺[Cu-1]⁻. Although this is an intriguing possibility, there is no spectroscopic evidence for the presence of [Cu-1]+ in the green, degraded sample (Figure 6). However, this might be expected, given that [Cu-1][PF₆] degrades over the course of several hours to form a diamagnetic species, releasing Cu(II).²¹ A previously reported crystal structure may support this disproportionation hypothesis. The structure of the copper complex of tris(4-nitrophenyl)corrole (CSD ID: IROGAY) has three independent corrole molecules in the asymmetric unit, and two of these molecules appear to form an ion pair (Figure S19).²³ Although this corrole was isolated as a red-brown species, the crystal was dark green, suggesting that the products from this chemical transformation are captured in the structure.

In an attempt to identify the reduction mechanism, we turned to spectroelectrochemistry. Beginning with the one-

electron-reduced corrole, the electrode was poised to regenerate neutral Cu-1. If the disproportionation mechanism were operative, it is expected that spectral signatures of the oxidized corrole [Cu-1]+ would be observed. However, the same spectral evolution is observed in the presence and absence of pyridine with no indication of the oxidized corrole (Figure S9). Next, neutral Cu-1 was oxidized, and spectral differences were observed for the sample with and without pyridine (Figure S10). In the absence of pyridine, the spectra are consistent with the chemically oxidized corrole using AgPF₆.²¹ The spectrum of the oxidation product with pyridine is distinct, but this could be due to the irreversibility of the oxidation with added pyridine. Therefore, the spectra could reflect the products from subsequent chemical reactivity rather than the oxidized species itself. The absence of a spectral signature is not a definitive assignment of the reduction mechanism. Indeed, the timescales of the spectroelectrochemical experiments (minutes to hours) and the reduction of Cu-1 in pyridine (weeks, see Figure 5B) are vastly different.

Collectively, these experiments shed light on the anomalous magnetic properties that have often been reported for copper corroles. Several studies have reported solvent-induced paramagnetism in DMF,^{23–25,67} pyridine,²⁴ and DMSO,²⁴ but this has largely been phenomenological with little chemical basis for this observation. One study proposed that these compounds are "spontaneously reduced" in coordinating solvents.²⁴ Other studies suggest that coordinating solvents shift the equilibrium $Cu(III)[Cor] \leq Cu(II)[Cor^{\bullet+}]$ toward the Cu(II) species.²⁵ Indeed, when EPR spectra similar to Figure 6 are reported, it is sometimes attributed to the presence of Cu(II)[Cor •+] in the sample. 74,75 Although it is true that Cu(II)[Cor*+] is present in the sample, the observed EPR signal is inconsistent with this species. The Cu(II) corrole radical cation could exist as either an antiferromagnetically coupled singlet (S = 0) or a ferromagnetically coupled triplet (S = 1). The sharp signals observed in Figure 6 are due to an axial doublet (S = 1/2), as corroborated by SQUID magnetometry and Evans method magnetic moment measurements. This study demonstrates that these anomalous EPR spectra are due to the presence of the one-electron reduced corrole in the sample, which likely arises from the use of wet benchtop solvents that contain adventitious water.

CONCLUSIONS

Metallocorroles have been utilized as catalysts to mediate a wide variety of chemical reactions. It is important to elucidate the electronic structure of these molecules and other key reaction intermediates to provide mechanistic insight for a given transformation. In many cases, it is not clear if redox processes occur at the metal or the ligand. This is especially true for first-row transition metal corrole complexes, as ligand non-innocence is pervasive for these molecules. Identifying the precise electronic structure of redox intermediates is important to gain mechanistic insight and then utilize that knowledge to develop superior catalysts.

This study has identified another key consideration when determining the electronic structure of transition metal corroles: the role of coordinating solvents. A series of complementary experiments has established that pyridine coordination to copper corroles modulates the coupling of the Cu(II) and corrole radical spins. Pyridine binding to Cu-1 induces a spin flip, changing the ground state from an antiferromagnetically coupled singlet to a ferromagnetically

coupled triplet. Although the triplet is stable for several days, this species undergoes a one-electron reduction to form the reduced corrole [Cu-1]⁻ over the course of several weeks. This process is accompanied by a dramatic color change from redbrown to green. Freshly prepared EPR samples using wet benchtop solvents give well-resolved spectral characteristic of an axial doublet, consistent with [Cu-1]⁻. This result suggests that water may be involved in the reduction mechanism. Together, these observations account for the solvent-induced paramagnetism and associated color changes observed for copper corroles in coordinating solvents.

Additional experiments are necessary to fully understand the role of pyridine in perturbing the electronic structure of Cu-1. One confounding observation is that pyridine changes the magnetic properties, but not the optical properties, of the copper corrole. Experiments to characterize pyridine binding and the interplay of optical and magnetic properties are necessary. Perhaps utilizing a ligand other than pyridine, or a ligand with distinct spectral signatures, could better characterize this phenomenon. Additionally, the mechanism by which triplet Cu-1 transforms into the one-electron-reduced derivative is unknown. LC-MS analysis of the reaction mixture could identify additional products and provide mechanistic insight for this process. Complementary techniques, such as emission spectroscopy, may also aid in the identification of modified pyridine products (e.g., bipyridine). However, these experiments are beyond the scope of the current study. We are currently working to address these outstanding questions in order to then utilize the coordination-induced spin-state switching of copper corroles for future applications.

Pyridine coordination in copper corroles changes the spin coupling between the metal and ligand. This is different from other transition metal corroles (e.g., Co), where a switch between an innocent and non-innocent corrole macrocycle is observed upon pyridine binding.⁶² A triplet ground state would engender reactivity that is distinct from the singlet state. Given the triplet ground state of Cu-1·pyr, this molecule will likely react more quickly with triplet species, such as molecular oxygen, relative to Cu-1. In this way, the scope of reactions mediated by copper corroles, which is currently limited to electrocatalytic proton reduction,⁶⁹ could be expanded. The observed transformation of the triplet to the one-electron reduced complex suggests that the pyridine adduct serves as an oxidant, and this reactivity could be leveraged for oxidation catalysis. In this vein, we are currently incorporating copper corroles into heme proteins as artificial metalloenzymes. By replacing the native heme cofactor with a corrole analogue, a well-defined five-coordinate copper corrole could be obtained with the heme-ligating histidine residue. While copper corroles have been previously incorporated into heme proteins, ^{76,77} the detailed electronic structure and potential activity of these substituted proteins have not yet been explored, and these conjugates may provide an inroad for the development of novel artificial metalloenzymes.

ASSOCIATED CONTENT

Supporting Information

The Supporting Information is available free of charge at https://pubs.acs.org/doi/10.1021/acs.inorgchem.2c02678.

Additional spectral data, ultrafast kinetic data, and DFT and TD-DFT results (PDF)

AUTHOR INFORMATION

Corresponding Authors

Christopher M. Lemon — Department of Chemistry and Chemical Biology, Harvard University, Cambridge, Massachusetts 02138, United States; Department of Chemistry & Biochemistry, Montana State University, Bozeman, Montana 59717, United States; ● orcid.org/0000-0001-9493-5488; Email: christopher.lemon1@montana.edu

Daniel G. Nocera — Department of Chemistry and Chemical Biology, Harvard University, Cambridge, Massachusetts 02138, United States; oorcid.org/0000-0001-5055-320X; Email: dnocera@fas.harvard.edu

Authors

- Andrew G. Maher Department of Chemistry and Chemical Biology, Harvard University, Cambridge, Massachusetts 02138, United States
- Bryce L. Anderson Department of Chemistry and Chemical Biology, Harvard University, Cambridge, Massachusetts 02138, United States
- Eric D. Bloch Department of Chemistry and Chemical Biology, Harvard University, Cambridge, Massachusetts 02138, United States; Present Address: Department of Chemistry and Biochemistry, University of Delaware, Newark, DE, 19716, United States; orcid.org/0000-0003-4507-6247
- Michael Huynh Department of Chemistry and Chemical Biology, Harvard University, Cambridge, Massachusetts 02138, United States
- Abie L. McCollar Department of Chemistry & Biochemistry, Montana State University, Bozeman, Montana 59717, United States

Complete contact information is available at: https://pubs.acs.org/10.1021/acs.inorgchem.2c02678

Notes

The authors declare no competing financial interest.

ACKNOWLEDGMENTS

This material is based upon work supported by a grant from the National Science Foundation (CHE-1855531). C.M.L. acknowledges the National Science Foundation's Graduate Research Fellowship Program and the College of Letters & Science at Montana State University for startup funds. We thank Dr. Kwabena Bediako for helpful discussions of the electrochemical data and Dr. Ryan Hadt for assistance with DFT calculations. Calculations were performed using the Odyssey cluster supported by FAS Research Computing. The authors thank Prof. Erik Grumstrup for allowing them to utilize the Shimadzu spectrometer and Prof. Thomas Livinghouse for providing pyridine- d_5 . We are grateful to Dr. Brian Tripet for acquiring additional NMR data. Funding for the Montana State University Chemistry and Biochemistry NMR Center was made possible in part by the MJ Murdock Charitable Trust (under award 2015066:MNL), the National Science Foundation (under award NSF-MRI:DBI-1532078 and NSF-MRI:CHE-2018388), and the Office of the Vice President for Research and Economic Development at MSU.

REFERENCES

- (1) Bousseksou, A.; Molnár, G.; Salmon, L.; Nicolazzi, W. Molecular Spin Crossover Phenomenon: Recent Achievements and Prospects. *Chem. Soc. Rev.* **2011**, *40*, 3313–3335.
- (2) Gütlich, P.; Garcia, Y.; Goodwin, H. A. Spin Crossover Phenomena in Fe(II) Complexes. *Chem. Soc. Rev.* **2000**, 29, 419–427.
- (3) Létard, J.-F.; Guionneau, P.; Goux-Capes, L.Towards Spin Crossover Applications. In *Spin Crossover in Transition Metal Compounds III*; Springer, 2004; Vol. 235, pp 221–249.
- (4) Aromí, G.; Aguilà, D.; Gamez, P.; Luis, F.; Roubeau, O. Design of Magnetic Coordination Complexes for Quantum Computing. *Chem. Soc. Rev.* **2012**, *41*, 537–546.
- (5) Matsumoto, T.; Newton, G. N.; Shiga, T.; Hayami, S.; Matsui, Y.; Okamoto, H.; Kumai, R.; Murakami, Y.; Oshio, H. Programmable Spin-State Switching in a Mixed-Valence Spin-Crossover Iron Grid. *Nat. Commun.* **2014**, *5*, 3865.
- (6) Shores, M. P.; Klug, C. M.; Fiedler, S. R.Spin-State Switching in Solution. In *Spin-Crossover Materials: Properties and Applications*; Halcrow, M. A., Ed.; John Wiley & Sons: Oxford, U.K., 2013; pp 281–301.
- (7) Gütlich, P.; Hauser, A.; Spiering, H. Thermal and Optical Switching of Iron(II) Complexes. *Angew. Chem., Int. Ed. Engl.* **1994**, 33, 2024–2054.
- (8) Ni, Z.; Shores, M. P. Magnetic Observation of Anion Binding in Iron Coordination Complexes: Toward Spin-Switching Chemosensors. *J. Am. Chem. Soc.* **2009**, *131*, 32–33.
- (9) Thies, S.; Bornholdt, C.; Köhler, F.; Sönnichsen, F. D.; Näther, C.; Tuczek, F.; Herges, R. Coordination-Induced Spin Crossover (CISCO) through Axial Bonding of Substituted Pyridines to Nickel–Porphyrins: σ -Donor versus π -Acceptor Effects. *Chem.—Eur J.* **2010**, *16*, 10074–10083.
- (10) Dommaschk, M.; Thoms, V.; Schütt, C.; Näther, C.; Puttreddy, R.; Rissanen, K.; Herges, R. Coordination-Induced Spin-State Switching with Nickel Chlorin and Nickel Isobacteriochlorin. *Inorg. Chem.* **2015**, *54*, 9390–9392.
- (11) Venkataramani, S.; Jana, U.; Dommaschk, M.; Sönnichsen, F. D.; Tuczek, F.; Herges, R. Magnetic Bistability of Molecules in Homogeneous Solution at Room Temperature. *Science* **2011**, *331*, 445–448.
- (12) Thies, S.; Sell, H.; Schütt, C.; Bornholdt, C.; Näther, C.; Tuczek, F.; Herges, R. Light-Induced Spin Change by Photodissociable External Ligands: A New Principle for Magnetic Switching of Molecules. *J. Am. Chem. Soc.* **2011**, *133*, 16243–16250.
- (13) Dommaschk, M.; Peters, M.; Gutzeit, F.; Schütt, C.; Näther, C.; Sönnichsen, F. D.; Tiwari, S.; Riedel, C.; Boretius, S.; Herges, R. Photoswitchable Magnetic Resonance Imaging Contrast by Improved Light-Driven Coordination-Induced Spin State Switch. *J. Am. Chem. Soc.* 2015, 137, 7552–7555.
- (14) Bröring, M.; Brégier, F.; Cónsul Tejero, E. C.; Hell, C.; Holthausen, M. C. Revisiting the Electronic Ground State of Copper Corroles. *Angew. Chem., Int. Ed.* **2007**, *46*, 445–448.
- (15) Alemayehu, A. B.; Gonzalez, E.; Hansen, L. K.; Ghosh, A. Copper Corroles are Inherently Saddled. *Inorg. Chem.* **2009**, 48, 7794–7799.
- (16) Thomas, K. E.; Conradie, J.; Hansen, L. K.; Ghosh, A. A Metallocorrole with Orthogonal Pyrrole Rings. *Eur. J. Inorg. Chem.* **2011**, 2011, 1865–1870.
- (17) Thomas, K. E.; Alemayehu, A. B.; Conradie, J.; Beavers, C. M.; Ghosh, A. The Structural Chemistry of Metallocorroles: Combined X-ray Crystallography and Quantum Chemistry Studies Afford Unique Insights. *Acc. Chem. Res.* **2012**, *45*, 1203–1214.
- (18) Alemayehu, A. B.; Hansen, L. K.; Ghosh, A. Nonplanar, Noninnocent and Chiral: A Strongly Saddled Metallocorrole. *Inorg. Chem.* **2010**, *49*, 7608–7610.
- (19) Pierloot, K.; Zhao, H.; Vancoillie, S. Copper Corroles: The Question of Noninnocence. *Inorg. Chem.* **2010**, *49*, 10316–10329.
- (20) Alemayehu, A.; Conradie, J.; Ghosh, A. A First TDDFT Study of Metallocorrole Electronic Spectra: Copper *meso*-Triarylcorroles Exhibit *Hyper* Spectra. *Eur. J. Inorg. Chem.* **2011**, 2011, 1857–1864.

- (21) Lemon, C. M.; Huynh, M.; Maher, A. G.; Anderson, B. L.; Bloch, E. D.; Powers, D. C.; Nocera, D. G. Electronic Structure of Copper Corroles. *Angew. Chem., Int. Ed.* **2016**, *55*, 2176–2180.
- (22) Lim, H.; Thomas, K. E.; Hedman, B.; Hodgson, K. O.; Ghosh, A.; Solomon, E. I. X-ray Absorption Spectroscopy as a Probe of Ligand Noninnocence in Metallocorroles: The Case of Copper Corroles. *Inorg. Chem.* **2019**, *58*, 6722–6730.
- (23) Bhattacharya, D.; Singh, P.; Sarkar, S. Synthesis, X-Structure and Solvent Induced Electronic State Tuning of *meso*-Tris(4-nitrophenyl)corrolato-copper Complex. *Inorg. Chim. Acta* **2010**, 363, 4313–4318.
- (24) Lu, G.; Lin, W.; Fang, Y.; Zhu, W.; Ji, X.; Ou, Z. Synthesis and Electrochemical Properties of *meso*-Phenyl Substituted Copper Corroles: Solvent Effect on Copper Oxidation State. *J. Porphyrins Phthalocyanines* **2011**, *15*, 1265–1274.
- (25) Brückner, C.; Briñas, R. P.; Krause Bauer, J. A. K. X-ray Structure and Variable Temperature NMR Spectra of [meso-Triarylcorrolato]copper(III). Inorg. Chem. 2003, 42, 4495–4497.
- (26) Lemon, C. M.; Halbach, R. L.; Huynh, M.; Nocera, D. G. Photophysical Properties of β -Substituted Free-Base Corroles. *Inorg. Chem.* **2015**, *54*, 2713–2725.
- (27) Fulmer, G. R.; Miller, A. J. M.; Sherden, N. H.; Gottlieb, H. E.; Nudelman, A.; Stoltz, B. M.; Bercaw, J. E.; Goldberg, K. I. NMR Chemical Shifts of Trace Impurities: Common Laboratory Solvents, Organics, and Gases in Deuterated Solvents Relevant to the Organometallic Chemist. *Organometallics* **2010**, *29*, 2176–2179.
- (28) Lemon, C. M.; Karnas, E.; Bawendi, M. G.; Nocera, D. G. Two-Photon Oxygen Sensing with Quantum Dot-Porphyrin Conjugates. *Inorg. Chem.* **2013**, *52*, 10394–10406.
- (29) Powers, D. C.; Anderson, B. L.; Nocera, D. G. Two-Electron HCl to H₂ Photocycle Promoted by Ni(II) Polypyridyl Halide Complexes. *J. Am. Chem. Soc.* **2013**, *135*, 18876–18883.
- (30) Bain, G. A.; Berry, J. F. Diamagnetic Corrections and Pascal's Constants. *J. Chem. Educ.* **2008**, *85*, 532–536.
- (31) Chilton, N. F.; Anderson, R. P.; Turner, L. D.; Soncini, A.; Murray, K. S. PHI: A Powerful New Program for the Analysis of Anisotropic Monomeric and Exchange-Coupled Polynuclear *d* and *f*-Block Complexes. *J. Comput. Chem.* **2013**, *34*, 1164–1175.
- (32) Evans, D. F. The Determination of the Paramagnetic Susceptibility of Substances in Solution by Nuclear Magnetic Resonance. J. Chem. Soc. 1959, 2003–2005.
- (33) Schubert, E. M. Utilizing the Evans Method with a Superconducting NMR Spectrometer in the Undergraduate Laboratory. J. Chem. Educ. 1992, 69, 62.
- (34) Becke, A. D. Density-Functional Exchange-Energy Approximation with Correct Asymptotic Behavior. *Phys. Rev. A* **1988**, *38*, 3098–3100.
- (35) Becke, A. D. A. New Mixing of Hartree–Fock and Local Density-Functional Theories. *J. Chem. Phys.* **1993**, 98, 1372–1377.
- (36) Becke, A. D. Density-Functional Thermochemistry. III. The Role of Exact Exchange. J. Chem. Phys. 1993, 98, 5648-5652.
- (37) Lee, C.; Yang, W.; Parr, R. G. Development of the Colle-Salvetti Correlation-Energy Formula into a Functional of the Electron Density. *Phys. Rev. B* **1988**, *37*, 785–789.
- (38) Frisch, M. J.; Trucks, G. W.; Schlegel, H. B.; Scuseria, G. E.; Robb, M. A.; Cheeseman, J. R.; Scalmani, G.; Barone, V.; Mennucci, B.; Petersson, G. A.; Nakatsuji, H.; Caricato, M.; Li, X.; Hratchian, H. P.; Izmaylov, A. F.; Bloino, J.; Zheng, G.; Sonnenberg, J. L.; Hada, M.; Ehara, M.; Toyota, K.; Fukuda, R.; Hasegawa, J.; Ishida, M.; Nakajima, T.; Honda, Y.; Kitao, O.; Nakai, H.; Vreven, T.; Montgomery, J. A., Jr.; Peralta, J. E.; Ogliaro, F.; Bearpark, M.; Heyd, J. J.; Brothers, E.; Kudin, K. N.; Staroverov, V. N.; Kobayashi, R.; Normand, J.; Raghavachari, K.; Rendell, A.; Burant, J. C.; Iyengar, S. S.; Tomasi, J.; Cossi, M.; Rega, N.; Millam, J. M.; Klene, M.; Knox, J. E.; Cross, J. B.; Bakken, V.; Adamo, C.; Jaramillo, J.; Gomperts, R.; Stratmann, R. E.; Yazyev, O.; Austin, A. J.; Cammi, R.; Pomelli, C.; Ochterski, J. W.; Martin, R. L.; Morokuma, K.; Zakrzewski, V. G.; Voth, G. A.; Salvador, P.; Dannenberg, J. J.; Dapprich, S.; Daniels, A.

- D.; Farkas, Ö.; Foresman, J. B.; Ortiz, J. V.; Cioslowski, J.; Fox, D. J. Gaussian 09; Revision D.01; Gaussian, Inc.: Wallingford, CT, 2009.
- (39) Lee, Y. S.; Ermler, W. C.; Pitzer, K. S. *Ab initio* Effective Core Potentials Including Relativistic Effects. I. Formalism and Applications to the Xe and Au Atoms. *J. Chem. Phys.* **1977**, *67*, 5861–5876.
- (40) Metz, B.; Stoll, H.; Dolg, M. Small-Core Multiconfiguration-Dirac-Hartree-Fock-Adjusted Pseudopotentials for Post-*d* Main Group Elements: Applications to PbH and PbO. *J. Chem. Phys.* **2000**, *113*, 2563–2569.
- (41) Barone, V.; Cossi, M. Quantum Calculation of Molecular Energies and Energy Gradients in Solution by a Conductor Solvent Model. *J. Phys. Chem. A* **1998**, *102*, 1995–2001.
- (42) Cossi, M.; Rega, N.; Scalmani, G.; Barone, V. Energies, Structures, and Electronic Properties of Molecules in Solution with the C-PCM Solvation Model. *J. Comput. Chem.* **2003**, *24*, 669–681.
- (43) Bauernschmitt, R.; Ahlrichs, R. Treatment of Electronic Excitations within the Adiabatic Approximation of Time Dependent Density Functional Theory. *Chem. Phys. Lett.* **1996**, 256, 454–464.
- (44) Casida, M. E.; Jamorski, C.; Casida, K. C.; Salahub, D. R. Molecular Excitation Energies to High-Lying Bound States from Time-Dependent Density-Functional Response Theory: Characterization and Correction of the Time-Dependent Local Density Approximation Ionization Threshold. *J. Chem. Phys.* **1998**, *108*, 4439–4449.
- (45) Stratmann, R. E.; Scuseria, G. E.; Frisch, M. J. An Efficient Implementation of the Time-Dependent Density-Functional Theory for the Calculation of Excitation Energies of Large Molecules. *J. Chem. Phys.* **1998**, *109*, 8218–8224.
- (46) Van Caillie, C.; Amos, R. D. Geometric Derivatives of Excitation Energies using SCF and DFT. *Chem. Phys. Lett.* **1999**, *308*, 249–255.
- (47) Scalmani, G.; Frisch, M. J.; Mennucci, B.; Tomasi, J.; Cammi, R.; Barone, V. Geometries and Properties of Excited States in the Gas Phase and in Solution: Theory and Applications of a Time-Dependent Density Functional Theory Polarizable Continuum Model. *J. Chem. Phys.* **2006**, *124*, 094107.
- (48) Lemon, C. M.; Hwang, S. J.; Maher, A. G.; Powers, D. C.; Nocera, D. G. Halogen Photoelimination from Sb^V Dihalide Corroles. *Inorg. Chem.* **2018**, *57*, 5333–5342.
- (49) Ngo, T. H.; Zieba, D.; Webre, W. A.; Lim, G. N.; Karr, P. A.; Kord, S.; Jin, S.; Ariga, K.; Galli, M.; Goldup, S.; Hill, J. P.; D'Souza, F. Engaging Copper(III) Corrole as an Electron Acceptor: Photo-induced Charge Separation in Zinc Porphyrin—Copper Corrole Donor—Acceptor Conjugates. *Chem.—Eur J.* 2016, 22, 1301–1312.
- (50) Magde, D.; Windsor, M. W.; Holten, D.; Gouterman, M. Picosecond Flash Photolysis: Transient Absorption in Sn(IV), Pd(II), and Cu(II) Porphyrins. *Chem. Phys. Lett.* **1974**, *29*, 183–188.
- (51) Hilinski, E. F.; Straub, K. D.; Rentzepis, P. M. Solvent Effects on the Relaxation Mechanism of Cu(II) Protoporphyrin. *Chem. Phys. Lett.* **1984**, *111*, 333–339.
- (52) Asano, M.; Kaizu, Y.; Kobayashi, H. The Lowest Excited States of Copper Porphyrins. *J. Chem. Phys.* **1988**, *89*, 6567–6576.
- (53) Drago, R. S. Physical Methods in Chemistry; W. B. Saunders: Philadelphia, 1977.
- (54) Renner, M. W.; Barkigia, K. M.; Fajer, J. Conformational Landscapes of Nonplanar Porphyrins: Superstructure, Ligation, Binding Pockets and Oxidation Effects in Cu(II) Porphyrins. *Inorg. Chim. Acta* 1997, 263, 181–187.
- (55) Orłowski, R.; Gryko, D.; Gryko, D. T. Synthesis of Corroles and Their Heteroanalogs. *Chem. Rev.* 2017, 117, 3102-3137.
- (56) Barata, J. F. B.; Neves, M. G. P. M. S.; Faustino, M. A. F.; Tomé, A. C.; Cavaleiro, J. A. S. Strategies for Corrole Functionalization. *Chem. Rev.* **2017**, *117*, 3192–3253.
- (57) Ghosh, A. Electronic Structure of Corrole Derivatives: Insights from Molecular Structures, Spectroscopy, Electrochemistry, and Quantum Chemical Calculations. *Chem. Rev.* **2017**, *117*, 3798–3881.
- (58) Ganguly, S.; Ghosh, A. Seven Clues to Ligand Noninnocence: The Metallocorrole Paradigm. Acc. Chem. Res. 2019, 52, 2003–2014.

Inorganic Chemistry Article pubs.acs.org/IC

- (59) Joyce, J. P.; Portillo, R. I.; Rappé, A. K.; Shores, M. P. Doublet Ground State in a Vanadium(II) Complex: Redox and Coordinative Noninnocence of Tripodal Ligand Architecture. Inorg. Chem. 2022, 61, 6376-6391.
- (60) Gross, Z.; Gray, H. B. How do Corroles Stabilize High Valent Metals? Comments Inorg. Chem. 2006, 27, 61-72.
- (61) Geier, G. R.; Chick, J. F. B.; Callinan, J. B.; Reid, C. G.; Auguscinski, W. P. A Survey of Acid Catalysts and Oxidation Conditions in the Two-Step, One-Flask Synthesis of Meso-Substituted Corroles via Dipyrromethanedicarbinols and Pyrrole. J. Org. Chem. 2004, 69, 4159-4169.
- (62) Ganguly, S.; Conradie, J.; Bendix, J.; Gagnon, K. J.; McCormick, L. J.; Ghosh, A. Electronic Structure of Cobalt-Corrole-Pyridine Complexes: Noninnocent Five-Coordinate Co(II) Corrole-Radical States. J. Phys. Chem. A 2017, 121, 9589-9598.
- (63) Ganguly, S.; Renz, D.; Giles, L. J.; Gagnon, K. J.; McCormick, L. J.; Conradie, J.; Sarangi, R.; Ghosh, A. Cobalt- and Rhodium-Corrole-Triphenylphosphine Complexes Revisited: The Question of a Noninnocent Corrole. Inorg. Chem. 2017, 56, 14788-14800.
- (64) Jiang, X.; Shan, W.; Desbois, N.; Quesneau, V.; Brandès, S.; Caemelbecke, E.; Osterloh, W. R.; Blondeau-Patissier, V.; Gros, C. P.; Kadish, K. M. Mono-DMSO Ligated Cobalt Nitrophenylcorroles: Electrochemical and Spectral Characterization. New J. Chem. 2018, 42, 8220-8229.
- (65) Quesneau, V.; Shan, W.; Desbois, N.; Brandès, S.; Rousselin, Y.; Vanotti, M.; Blondeau-Patissier, V.; Naitana, M.; Fleurat-Lessard, P.; Van Caemelbecke, E.; Kadish, K. M.; Gros, C. P. Cobalt Corroles with Bis-Ammonia or Mono-DMSO Axial Ligands. Electrochemical, Spectroscopic Characterizations and Ligand Binding Properties. Eur. J. Inorg. Chem. 2018, 2018, 4265-4277.
- (66) Osterloh, W. R.; Quesneau, V.; Desbois, N.; Brandès, S.; Shan, W.; Blondeau-Patissier, V.; Paolesse, R.; Gros, C. P.; Kadish, K. M. Synthesis and the Effect of Anions on the Spectroscopy and Electrochemistry of Mono(dimethyl sulfoxide)-Ligated Cobalt Corroles. Inorg. Chem. 2020, 59, 595-611.
- (67) Ye, L.; Ou, Z.; Fang, Y.; Song, Y.; Li, B.; Liu, R.; Kadish, K. M. Effect of NO₂ Substitution and Solvent on UV-Visible Spectra, Redox Potentials and Electron Transfer Mechanisms of Copper β -Nitrotriarylcorroles. Proposed Electrogeneration of a Cu(I) Oxidation State. J. Porphyrins Phthalocyanines 2016, 20, 753-765.
- (68) Zhang, W.; Lai, W.; Cao, R. Energy-Related Small Molecule Activation Reactions: Oxygen Reduction and Hydrogen and Oxygen Evolution Reactions Catalyzed by Porphyrin- and Corrole-Based Systems. Chem. Rev. 2017, 117, 3717-3797.
- (69) Lei, H.; Fang, H.; Han, Y.; Lai, W.; Fu, X.; Cao, R. Reactivity and Mechanism Studies of Hydrogen Evolution Catalyzed by Copper Corroles. ACS Catal. 2015, 5, 5145-5153.
- (70) Li, M.; Niu, Y.; Zhu, W.; Mack, J.; Fomo, G.; Nyokong, T.; Liang, X. A₂B Type Copper(III)corroles Containing Zero-to-Five Fluorine Atoms: Synthesis, Electronic Structure and Facile Modulation of Electrocatalyzed Hydrogen Evolution. Dyes Pigm. 2017, 137, 523-531.
- (71) Sudhakar, K.; Mahammed, A.; Chen, Q.-C.; Fridman, N.; Tumanskii, B.; Gross, Z. Copper Complexes of CF₃-Substituted Corroles for Affecting Redox Potentials and Electrocatalysis. ACS Appl. Energy Mater. 2020, 3, 2828-2836.
- (72) Gao, Y.; Liu, J.; Wang, M.; Na, Y.; Åkermark, B.; Sun, L. Synthesis and Characterization of Manganese and Copper Corrole Xanthene Complexes as Catalysts for Water Oxidation. Tetrahedron 2007, 63, 1987-1994.
- (73) Garrido-Barros, P.; Funes-Ardoiz, I.; Drouet, S.; Benet-Buchholz, J.; Maseras, F.; Llobet, A. Redox Non-innocent Ligand Controls Water Oxidation Overpotential in a New Family of Mononuclear Cu-based Efficient Catalysts. J. Am. Chem. Soc. 2015,
- (74) Yadav, P.; Sankar, M.; Ke, X.; Cong, L.; Kadish, K. M. Highly Reducible π -Extended Copper Corroles. Dalton Trans. 2017, 46, 10014-10022.

- (75) Haas, M.; Gonglach, S.; Müllegger, S.; Schöfberger, W. Synthesis and Characterization of meso-Substituted A2B Corroles with Extended π -Electronic Structure. Monatsh. Chem. 2018, 149, 773 - 781.
- (76) Bröring, M.; Brégier, F.; Burghaus, O.; Kleeberg, C. A Biomimetic Copper Corrole-Preparation, Characterization, and Reconstitution with Horse Heart Apomyoglobin. Z. Anorg. Allg. Chem. 2010, 636, 1760-1766.
- (77) Lemon, C. M.; Marletta, M. A. Designer Heme Proteins: Achieving Novel Function with Abiological Heme Analogues. Acc. Chem. Res. 2021, 54, 4565-4575.

□ Recommended by ACS

A GdIII-Based Spin Label at the Limits for Linewidth **Reduction through Zero-Field Splitting Optimization**

Daniel Ossadnik, Adelheid Godt, et al.

DECEMBER 16, 2022

INORGANIC CHEMISTRY

READ 2

Single-Molecule Magnetism in Linear Fe(I) Complexes with **Aufbau and Non-Aufbau Ground States**

Rishu Khurana and Md. Ehesan Ali

SEPTEMBER 21, 2022

INORGANIC CHEMISTRY

READ **C**

Low-Coordinate Erbium(III) Single-Molecule Magnets with **Photochromic Behavior**

Katarzyna Rogacz, Dawid Pinkowicz, et al.

OCTOBER 05, 2022

INORGANIC CHEMISTRY

READ **C**

Insights into the Spin Dynamics of Mononuclear Cerium(III) Single-Molecule Magnets

Franz A. Mautner, Silvia Gómez-Coca, et al.

JULY 11, 2022

INORGANIC CHEMISTRY

READ 2

Get More Suggestions >